12th IEA Heat Pump Conference 2017

Ejector refrigeration system driven by renewable energy and waste heat

Mark Anthony Redo[a*], Menandro Berana[b], Kiyoshi Saito[a]

[a]*Waseda University, Okubo Shinjuku, Tokyo 169-8555, Japan*
[b]*University of the Philippines, Diliman, Quezon City 1101, Philippines*

Abstract

Ejector cooling systems utilize low-grade thermal energy from waste heat or renewable energy sources replacing the power consuming compressor of the conventional vapor compression system. Thus, it offers solution in reducing primary energy consumption and realization of energy conservation. The abundance of Philippine heat sources like solar, geothermal, biomass and recoverable industrial waste heat were introduced possessing high potential of utilization and application. The amount of heat input required to produce a fixed 100 kW cooling capacity for industrial or commercial application was projected for varying the primary vapor flow temperature at the outlet of the generator from 60ºC to 100ºC. This generating temperature includes a 3ºC superheat. The evaporating temperature was varied at 5ºC, 10ºC and 15ºC. The condensing temperature was maintained at 40ºC considering the ambient temperature of the country. R717, R134a, R152a and R290 were each studied and employed as working fluids for the system.

Mathematical modelling was established where governing principles of Thermodynamics and conservation equations were employed to elementary control volumes of the ejector sections. Isentropic and irreversible processes were considered and entropy generation was accounted from frictional losses. An ejector geometry is computed to work optimally for each simulation with a given set of working conditions and working fluid. Results have shown the relationship of entrainment ratio, COP and area ratio as important performance indicators which are highly dependent on the working conditions, fluid properties and ejector geometry.

Keywords: Ejector; cooling system; solar; biomass; waste heat

* Corresponding author. Tel.: +81-3-5286-3259; fax: +81-3-5286-3259.
E-mail address: m.redo@moegi.waseda.jp.

Nomenclature

A : cross-sectional area, m^2
C : correction parameter for friction factor
D : diameter, m
f : friction factor
h : specific enthalpy, $kJ \cdot kg^{-1}$
irr : irreversible
isen : isentropic
L_m : mixing chamber length, m
$\dot{m}_m$: mixed or total flow, kg/s
$\dot{m}_p$: primary mass flow rate, kg/s
$\dot{m}_s$: secondary mass flow rate, kg/s
P : pressure, kPa
py : primary flow at y-y
Q_c : condensing heat, kW
Q_e : refrigerating capacity, kW
Q_g : generating heat, kW
Re : Reynolds number
sy : secondary flow at y-y
T : temperature, C
u : velocity, m/s
v : specific volume, m^3/kg
θ_{con} : converging angle
θ_{div} : diverging angle
W_p : pump work
ω : entrainment ratio
1-6 : state points

1. Introduction

Modern industrial civilization greatly relies on fossil fuels as the primary energy source. However, this natural resource is geologically formed in the past and is subject to depletion [1]. Its near-term peak and terminal decline associated with the rapid increase of global population are being forecasted by several scientists and engineers [2]. In the Philippines, 74.6% of the power generation source comes from fossil fuels such as oil, coal and natural gas based on the 2015 statistics [3]. Large portion of this generated power goes to residential, industrial and commercial sectors which is primarily used for recreation, space cooling, air conditioning and refrigeration applications. On the one hand, the Philippines highly depends on power consuming vapor refrigeration systems which consume great amount of primary energy. On the other hand, abundant low-grade thermal energy resources are locally available and can be utilized for a heat-driven cooling system. Low-grade thermal energy, also referred to as the secondary or waste heat, pertains to a low temperature heat having less exergy density and cannot be efficiently converted through a conventional method. This means that the category is for the heat below 370°C which does not work in a steam Rankine cycle [4]. The sources could be renewable such as geothermal, solar, biomass products or waste heat from industrial processes.

Philippines is abundant with low energy resources, yet big amount are still untapped and wasted. The country is the second largest producer of geothermal energy next to United States based on the installed capacity [5]. However, aside from high-enthalpy being exploited for electrical generation, there is a significant amount of low-enthalpy geothermal reservoirs that are still unutilized. The Philippine Department of Energy on their geothermal explorations has mapped 23 local areas with low-grade geothermal pool ranging from 60°C to 100°C [3]. Substantial amount of solar radiation is also being received by the country having located just above the equator and with longer summer period. A solar irradiation mapping is being conducted both by the local and foreign institutions. In support to the satellite information, ground irradiance data are measured in specific places which gave irradiation ranging from 1,644 to 1,987 kWh/m^2yr [6]. In terms of biomass, a large quantity of these products are available since Philippines is an agricultural country where 40% of the total population is engaged in this industry. In fact, it boasts its 2^{nd} ranking on the largest producer of coconut in the world, and 8^{th} for rice [7]. Baconguis [8] has specified and reported big amount of each abandoned biomass product. When it comes to waste heat, a great number of industries signifies its value. The data from the World Bank Databank, 2010 reference, has shown that the Philippines is the 24^{th} largest manufacturing sector in the world out of 214

countries. These manufacturing companies basically use equipment and machines for their production requirements, and therefore generating low-temperature or waste heat as a by-product which is just being thrown out to the environment. The study of Redo et al. [9] has presented a substantial recoverable waste heat from an actual boiler flue gas data of a production plant in the Philippines.

A low-grade heat-driven cooling system can therefore be explored and applied as a way to address the energy crisis and bigger primary energy demands for cooling needs. Ejector refrigeration system (ERS) has proven to be more advantageous than other heat-driven systems as it satisfactorily works at a lower heat source temperature and there is no limit to a choice of working fluid to use. Furthermore, the ejector being the key component has no moving parts, structurally simple, reliable and has low initial and maintenance costs [10]. However, there is foremost a necessity to properly model the ejector to come up with the desired cooling output. A large number of studies which present various ERS modelling methods and results are available. Wide researches have focused on a single phase ejectors but there is a very limited modelling of two-phase ejectors [11]. In addition, most of the available papers dealt with isentropic processes for expansion and compression. Thus, this work has considered an irreversible process and two-phase flow modelling of the ejector. Wide range of working conditions are employed and four different working fluids (R717, R134a, R152a and R290) are tested in search for an optimum performance for ERS and applicability for available low-grade heat sources.

2. System Modelling

The schematic diagram in Figure 1a shows the standard components and cycle of a single ERS. The corresponding T-s graph is illustrated in Figure 1b. Referring to both illustrations, the low-grade heat energy (Q_g) enters the vapor generator and gives off heat to the refrigerant coming from the pump which is vaporized after passing through the heat exchanger. At a high temperature and pressure condition, this primary flow ($\dot{m}_p$) enters the converging-diverging nozzle of the ejector. It exits at a very low pressure but at supersonic velocity. This motive or primary flow produces dragging or entrainment for the suction or secondary flow ($\dot{m}_s$) which comes from the evaporator. Both flows are mixed together then shock wave is instigated along the mixing. This mixed flow ($\dot{m}_m$) passes through the diffuser where recompression happens and the kinetic energy is converted back to pressure energy. It then enters the condenser where heat flux (Q_c) is rejected. Mixed flow is separated where some part is pumped back to the generator as the primary flow, and the other part which is the secondary flow is expanded towards the evaporator where cooling is produced (Q_e).

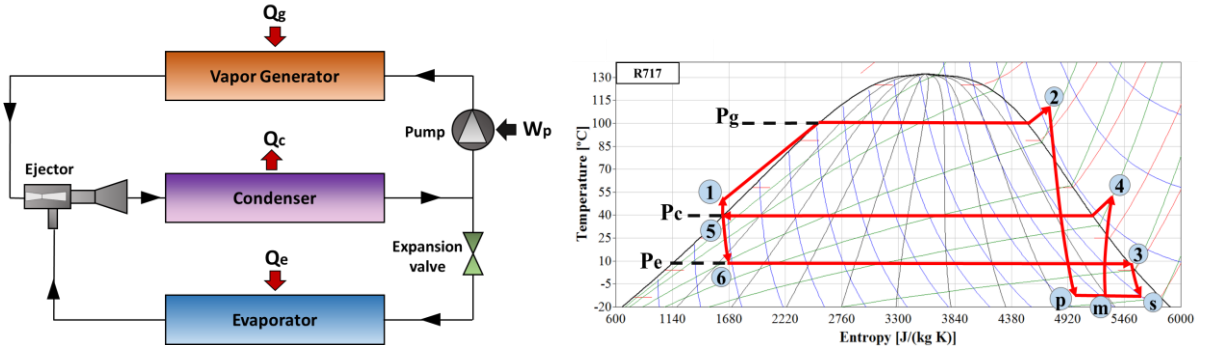

Fig. 1. (a) Ejector Refrigeration Cycle Schematic Diagram, (b) T-s graph

Energy balance is employed for the vapor generator, condenser and the evaporator quantifying the heat absorbed and rejected under steady state operating conditions expressed from Eqns. 1 to 3.

$$Q_g = \dot{m}_p \left(h_2 - h_1 \right) \tag{1}$$

$$Q_c = \dot{m}_m \left(h_4 - h_5 \right) \tag{2}$$

$$Q_e = \dot{m}_s \left(h_3 - h_6 \right) \tag{3}$$

Important parameters to characterize the ejector performance are calculated and observed. One of which is the entrainment ratio (ω) defined as the ratio of the secondary mass flow rate and the primary mass flow rate as stated in Eqn. 4.

$$\omega = \frac{\dot{m}_s}{\dot{m}_p} \tag{4}$$

The coefficient of performance (COP) of a standard and single ERS is defined as the ratio of the refrigerating capacity over the heat absorbed from a low-grade heat source and the pump work as shown in Eqn. 5. However, pump work is neglected due to its small value. In Eqn. 6, COP can also be expressed as a function of the entrainment ratio and enthalpy differences on the evaporator and the vapor generator.

$$COP = \frac{Q_e}{Q_g + W_p} \tag{5}$$

$$COP = \frac{\dot{m}_s \Delta h_e}{\dot{m}_p \Delta h_g} = \omega \left(\frac{\Delta h_e}{\Delta h_g} \right) \tag{6}$$

3. Ejector Modelling

Ejector is the heart of the ERS which performs the entrainment, mixing and compression to produce cooling. It must therefore be designed properly. Basic components of ERS are (a) primary converging-diverging nozzle, (b) pre-mixing section, (c) mixing chamber and (d) diffuser. Each section is carefully modelled where the fundamental concepts of thermodynamics and conservation equations are employed. The fluid properties of each of the refrigerant are taken from REFPROP 9.1 [12] which makes use of the data from the National Institute of Standards and Technology (NIST).

Prior to the mathematical modelling, assumptions are defined as follows: (a) Fluid flow is homogenous having the same properties at every point; (b) steady-state and one-dimensional flow; (c) adiabatic flow is considered where there is no heat gain or loss; (d) irreversibility is due to frictional losses; (e) phase-change is accounted; (f) two-phases are assumed to have complete interaction flowing in equilibrium.

3.1. Converging-diverging nozzle

Conversion from pressure energy to kinetic energy occurs as the fluid expands inside the primary nozzle. Supersonic speed is attained at a low-pressure in two-phase region at the exit of the nozzle. For the modelling, this converging-diverging nozzle is divided into elementary control volumes where every section corresponds to a very small temperature decrement that sufficiently accounts for the frictional losses.

For the isentropic process, the entropy during expansion is represented by a red line shown in Figure 2. Meanwhile, the path of an irreversible expansion process is traced in blue line which goes to the right. Since adiabatic process is assumed (Q_{cv} = 0), there is no heat gain or loss in the system. The irreversibility or the generated entropy is mainly caused by the frictional losses.

The conservation equations for energy, mass and momentum employed in the modelling are presented in Eqn. 7, Eqn. 8 and Eqn. 9 respectively.

$$dh + d\left(\frac{u^2}{2}\right) = 0 \tag{7}$$

$$\frac{u_1 A_1}{v_1} = \frac{u_2 A_2}{v_2} \tag{8}$$

$$-vdP = d\left(\frac{u^2}{2}\right) + 2f\frac{u^2}{D}dz \tag{9}$$

The specific volume which is the inverse of density is simply carried out through REFPROP 9.1 for two-phase flow. For the friction factor f, Blasius-type is used adopted from the study of Berana [13].

$$f = CRe^{-n} \tag{10}$$

Numerous studies relate the friction factor with the Reynolds number (Re). Detailed analyses with experimental data are concluded by Joseph and Yang [14] which yielded the following relationship:

3050 < Re < 240000, C = 0.351 and n = 0.225;

Re > 240000, C = 0.118 and n = 0.165

The Reynolds number is the ratio of inertial force and the viscous force. The viscosity used is a function of quality which is similar to thermodynamic properties [15].

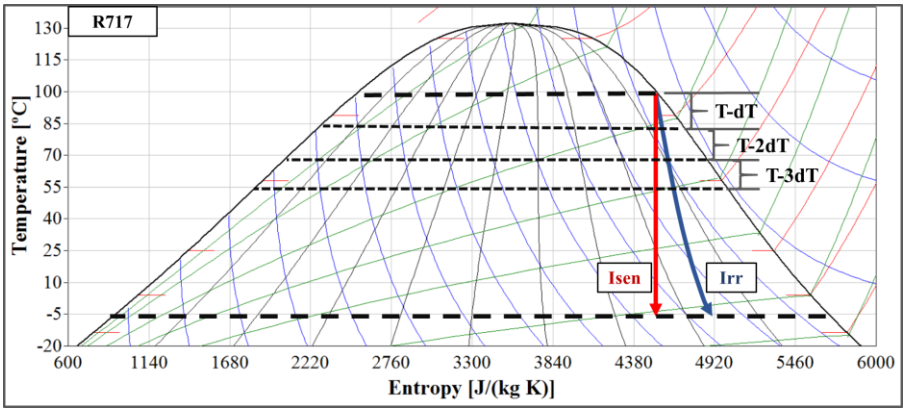

Fig. 2. Isentropic and irreversible nozzle expansion in two-phase region

The Conservation of Energy and Momentum of Eqn. 7 and Eqn. 9 are combined which results to Eqn. 11.

$$dh = vdP + 2f\frac{u^2}{D}dz \tag{11}$$

The differential length (dz) which denotes the length of the control volume (L) and the corresponding diameter (D) are derived and obtained for both the converging and the diverging sections portrayed in Figure 3.

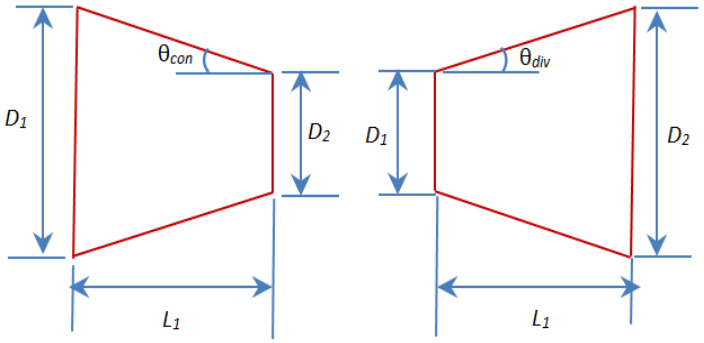

Fig. 3. (a) Converging section, (b) diverging section

The equations for the converging and diverging sections are expressed in Eqn. 12 and Eqn. 13 respectively.

$$D_2 = D_1 - 2L\tan\theta_{con} \tag{12}$$

$$D_2 = D_1 + 2L\tan\theta_{div} \tag{13}$$

The converging angle is fixed at 60º which produced the highest nozzle efficiency according to the study of Redo et al. [16] while the diverging angle is set at 8º based on the recommendation of ASHRAE [17] and ESDU [18].

3.2. Pre-mixing zone

The fluid at supersonic velocity continuously expands after exiting the primary nozzle as illustrated in Figure 4. From point x-x to point y-y the expansion takes the form of the diverging section where the same numerical technique is also extended. This occurrence gives way for the entrainment of the secondary flow which happens for two reasons. First, there is a pressure difference between the two flows. Expansion of the primary flow created a very low pressure region than the secondary flow at the evaporator's pressure which causes depression for two pressure streams [19]. Second, there is an extreme velocity difference for the two flows. The supersonic speed of the primary flow generates viscous dragging effect to the secondary flow [20, 21].

The extreme difference of fluid and flow properties creates a barrier implying no energy, momentum and mass exchange for both flows. The dividing shear layer yields a hypothetical converging nozzle for the secondary flow [22]. Elemental control volume is similarly applied. Both expanding streams are simultaneously solved numerically until the secondary reaches sonic velocity and the pressure equalizes [23].

3.3. Mixing Chamber

Random mixing of two flows commence at a uniform pressure from point y-y until a homogenous and fully mixed flow is obtained at point m-m as shown in Figure 4. Sufficient mixing length must be allocated to facilitate a complete mixing. The experimentally validated assumption of Sankarlal and Mani [24] is mathematically adapted recommending that the mixing length is ten times the chamber diameter ($L_m = 10\ D_m$).

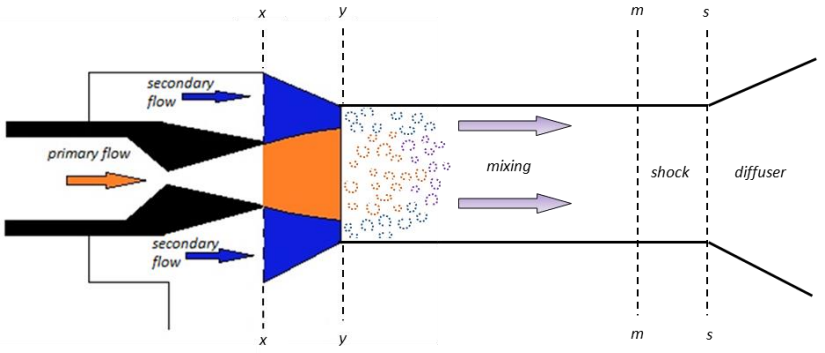

Fig. 4. The pre-mixing to mixing zone

The properties of the fully mixed flow are drawn from the combined Conservation of Mass and Momentum equations expressed in Eqn. 14.

$$P_y A_{py} + u_{py}\dot{m}_p + P_y A_{sy} + u_{sy}\dot{m}_s = P_m A_m + u_m(\dot{m}_p + \dot{m}_s) \tag{14}$$

The study of Keenan et al. [25] has experimentally demonstrated a better performance for a constant-pressure ejector. Velocity is computed through the simplified expression in Eqn. 15. Quality is subsequently incorporated for two-phase flow and is numerically solved.

$$u_m = \frac{P_y A_{py} + u_{py}\dot{m}_p + P_y A_{sy} + u_{sy}\dot{m}_s - P_y A_m}{\dot{m}_p + \dot{m}_s} \tag{15}$$

The instigation of shock wave is brought about by the fluid compressibility at its supersonic velocity. Pressure and temperature abruptly increase while the velocity drops down to subsonic. The properties at the shock front are determined by the intersection of Fanno and Rayleigh lines from the plotted locus of states for the vapor quality of the corresponding conservation equations. Moreover, the shock length is small and can therefore be accounted to the total mixing length [24].

3.4. Diffuser

As the mixed flow passes through the diffuser, its kinetic energy is converted back to pressure energy. The numerical technique employed for the diverging section of the primary nozzle is similarly carried out. However, stepwise iteration is conducted for every control volume where temperature is incremented since the process is compression. The outlet state of the diffuser becomes the inlet of the condenser.

4. Results and Discussion

Formulations and mathematical procedures are carefully performed for the modelling of the ERS. After the numerical program is completed, parameters are set accordingly. Heat input (Q_g) requirement from the low-grade heat source is investigated to produce a fixed 100 kW cooling capacity (Q_e). Condensing temperature (T_c) is maintained at 40°C considering the Philippine ambient temperature. Generating temperature (T_g) of the refrigerant is in the range from 60°C to 100°C and a 3°C superheat is added. Meanwhile, the evaporating temperature (T_e) is varied at 5°C, 10°C and 15°C. Simulation was conducted for every set of condition for four different working fluids such as R717, R134a, R152a and R290.

The behavior of entrainment ratio (ω) as an important parameter is observed along the variation of generating temperature shown in Figure 5.

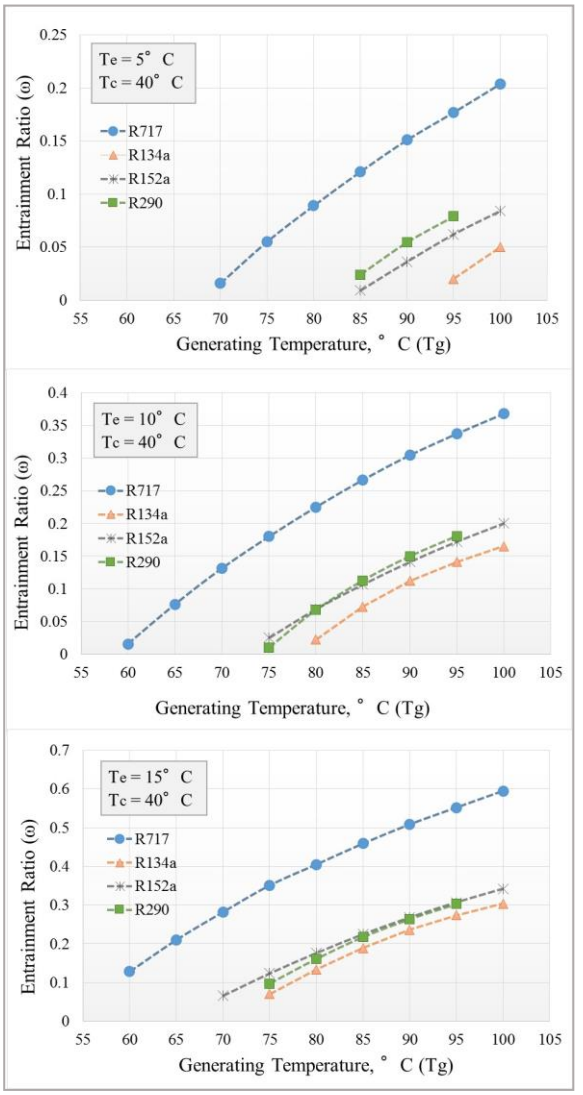

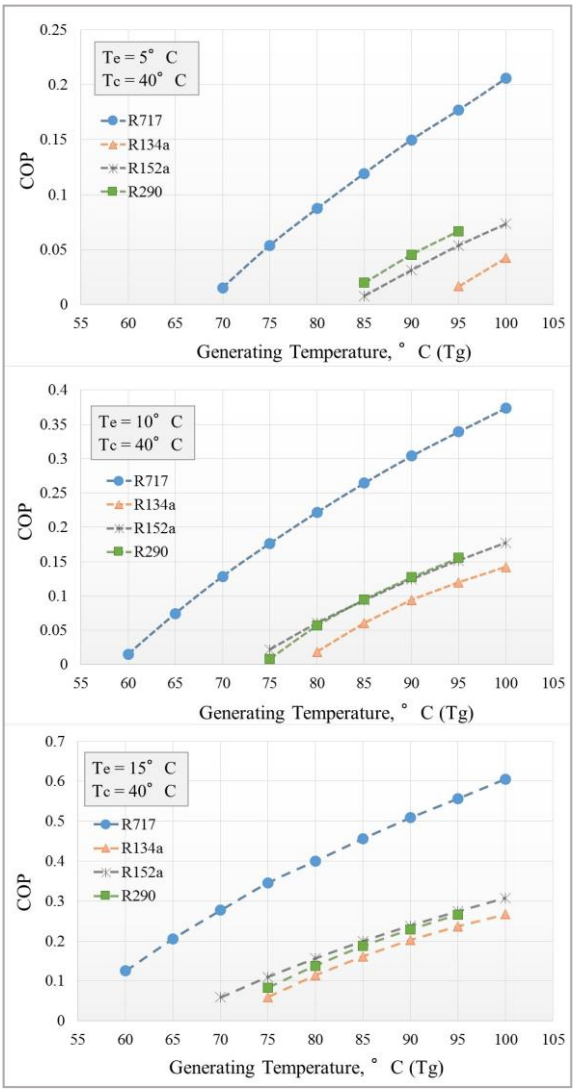

Fig. 5. Effect of T_g and T_e to entrainment ratio

Fig. 6. Effect of T_g and T_e to COP

At a fixed evaporating temperature, the entrainment ratio generally increases along the increment of the generating temperature for all the working fluids. The choking phenomenon explains that at a higher generating temperature or pressure, smaller amount of primary mass flow rate or motive flow is required to entrain a fixed amount of secondary mass flow rate or suction flow giving a higher entrainment ratio. In reverse, as the generating temperature drops continually, it reaches a point where the motive flow rate closely equalizes to the suction flow rate and no entrainment is therefore produced. Comparing the three graphs in Figure 5, another observation is drawn out. As the evaporating temperature increases, entrainment ratio also increases since higher evaporating pressure requires smaller amount of motive flow. Therefore, lower evaporating temperature necessitates higher generating temperature to induce choking or entrainment.

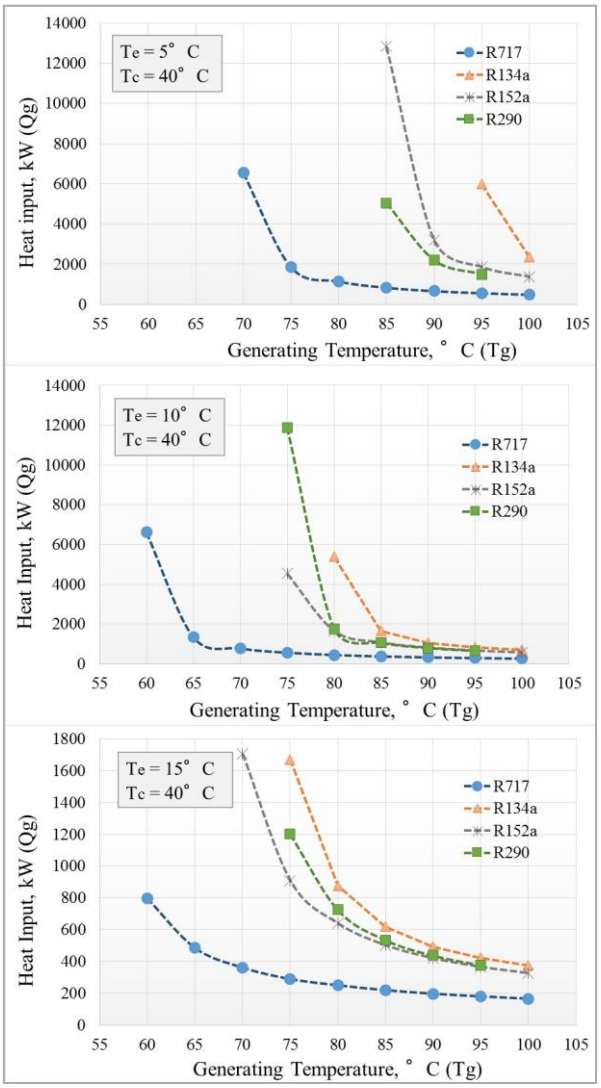

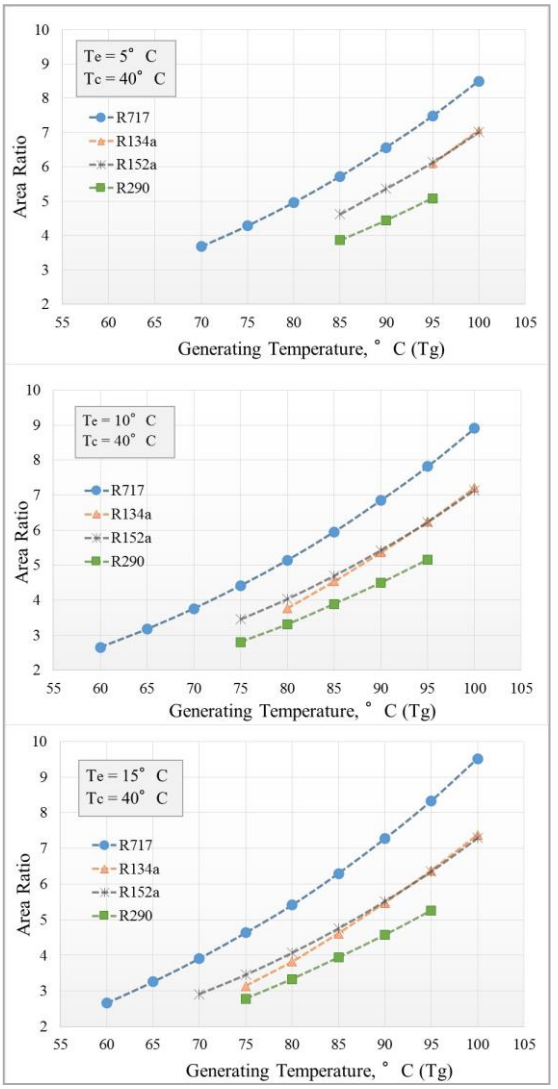

Fig. 7. Heat input requirement for varying the generating temp.

Fig. 8. Effect on area ratio for varying the generating temp.

The profiles of the coefficient of performance (COP) are portrayed on the graphs in Figure 6. They are observably similar to the profiles of the entrainment ratio. The reason for this is that the COP is highly dependent on the ratio of the mass flow rates expressed in Eqn. 6. Additionally, the refrigerating capacity is fixed, and so the COP solely relies to the change in enthalpy at the vapor generator which is very small and minor. Therefore, COP resembles closely with the entrainment ratio and increases along with the generating temperature. Comparing the three graphs, higher generating temperature is required for a lower evaporating temperature to facilitate cooling. This goes with the reason for entrainment explained earlier. R134a offers a lower COP while R152a and R290 have closely similar path of performance. However, R290 is limited to up to 95°C generating temperature operation since its critical temperature is 96.7°C. R717 (ammonia) yielded the highest COP out of all the conditions and obtained maximum at 0.6. It can operate at the lowest generating temperature as well.

The corresponding heat input (Q_g) requirement for a cooling capacity of 100 kW is projected along the variation of generating temperature shown in Figure 7. This heat absorbed by the primary flow for vaporization is a function of mass flow rate and the enthalpy difference between the outlet and the inlet of the vapor generator. As illustrated on the graphs, this heat input decreases as the generating temperature increases for all the fluids. Foremost, this is because the latent heat gets narrower and smaller as the generating temperature goes towards the critical region. Second, less amount of primary mass flow rate is required at a higher generating temperature for a fixed value of secondary mass flow rate. However, higher generating temperature means higher temperature requirement from the low-grade heat source. Looking at the variation of the evaporating temperature when taking a generating temperature at fixed value, the heat input requirement is lower for all fluids as the evaporating temperature goes up. R134a, R152a and R290 demands closed amount of Q_g especially for T_e at 10°C and 15°C and T_g from 85°C to 100°C. R717 emerged to requiring the lowest Q_g for all sets of conditions.

The area ratio referred to as the ratio of the cross-sectional areas of the mixing chamber and the primary nozzle's throat is depicted in Figure 8. This non-dimensional parameter significantly relates motive flow to suction flow entrainment and the mixing of two flows with the geometrical area. Ejector with higher area ratio produces better entrainment ratio while one with lower area ratio experiences higher losses which consequently yields comparatively lower entrainment ratio [26]. Graphs show that the area ratio rises along the increment of generating temperature. This logically comes with the relationship of entrainment ratio and generating temperature. Higher area ratio means higher entrainment and vice versa. This also explains why R717 has the highest area ratio among the four refrigerants.

The modelling yields the optimized ejector geometry for very set of working conditions per working fluid. The ejector geometric dimensions are specified in Table 1 for each refrigerant at its minimum and maximum COP with an ejector profile pattern in Figure 9.

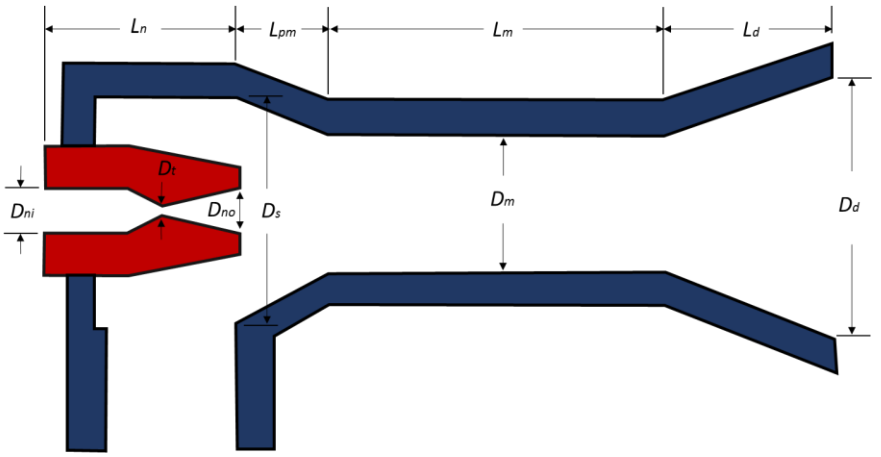

Fig. 9. Ejector profile

Table 1. Ejector dimensions (in millimeters) for the minimum and maximum COP of every working fluid; T_g and T_e are in degree C

Working Fluid	COP	Tg	Te	Dp	Dt	Dnexit	Dsec	Dm	Ddif	Lt	Lnozzle	Lbm	Lm	Ldiff	Ltotal
R717	0.015	70.0	5.0	250.9	37.5	49.3	96.7	71.6	250.1	61.7	104.4	37.9	716.2	506.0	1364.6
	0.606	100.0	15.0	28.1	4.3	6.4	64.5	13.3	69.7	6.9	14.4	5.2	133.4	159.8	312.8
R134a	0.017	95.0	5.0	203.6	55.6	90.1	150.1	133.9	245.0	43.1	170.3	73.8	1338.5	315.2	1897.8
	0.267	100.0	15.0	47.1	13.1	19.9	87.8	35.0	68.7	9.9	34.9	15.6	350.2	95.4	496.1
R152a	0.008	85.0	5.0	378.2	85.6	124.3	183.8	180.4	367.4	85.0	228.6	97.1	1803.9	530.2	2659.8
	0.307	100.0	15.0	49.5	11.6	17.1	89.6	30.8	67.7	11.0	31.3	13.5	308.2	104.6	457.6
R290	0.020	85.0	5.0	215.4	46.8	61.9	115.8	89.6	224.3	49.0	107.1	46.2	896.4	382.0	1431.8
	0.266	95.0	15.0	51.4	11.6	15.3	77.6	26.0	65.2	11.6	25.4	11.2	260.5	111.0	408.1

5. Conclusion

This study has presented the effect of varying the generating and evaporating temperatures at fixed condensing temperature and cooling capacity. Entrainment ratio, COP and area ratio are three important parameters which relate one to another. The values and trends of these ERS performance indicators vary according to the set of working conditions and refrigerants. Moreover, the projected ejector geometry works optimally for the specified set of working conditions and fluid. Amongst the four refrigerants, R717 (ammonia) emerged to offer a large range of generating temperature choices and the highest performance.

With the mathematical model suggesting an optimized ejector geometry, a set of working conditions can be selected to match the characteristics of available low-grade heat to the cooling requirement giving the desired performance for the heat-driven ERS. The next line of work leads to verifying the mathematical results particularly on the actual utilization of the abundant renewable and waste heat resources of the Philippines.

References

[1] Campbell CJ. Recognising the second half of the oil age. Environmental Innovation and Societal Transitions 2013;9:13-17.
[2] Hook M. Depletion rate analysis of fields and regions: A methodological foundation. Fuel 2014;121:95-108.
[3] Philippine Department of Energy (DOE) 2010-2015, Energy Center, Rizal Drive, Bonifacio Global City, Taguig City, Philippines 1632, http://www.doe.gov.ph/
[4] Chen H. Converting low-grade heat into electrical power. University of South Florida 2013.
[5] Matek B. Geothermal Energy Association. Annual U.S. & Global Geothermal Power 2016
[6] MacDonald M., 2015. “Philippine solar resource characterization, challenges and implications for the sector,” ASEF Asia Solar Energy Forum.
[7] Food and Agriculture Organization of the United Nations, FAO statistics.
[8] Baconguis R., 2007. “Abandoned biomass resource statistics in the Philippines,” 10th National Convention on Statistics (NCS).

[9] Redo M.A., Salvio B., Bongat R., Berana M., 2012. "Recovering waste heat from boiler flue gas for ejector refrigeration application," Philippine Society of Mechanical Engineers 60th Annual National Convention.
[10] Vidal H, Colle S. Simulation and economic optimization of a solar assisted combined ejector-vapor compression cycle for cooling applications. Applied Thermal Engineering 2010;30:478-486.
[11] Besagni G, Mereu R, Inzoli F. Ejector refrigeration: A comprehensive Review. Renewable and Sustainable Energy Reviews 2016;53:373-407.
[12] NIST Standard Reference Database 23, NIST Thermodynamics and Transport Properties of Refrigerants and Refrigerant Mixtures, REFPROP, Version 9.1 (2013).
[13] Berana M.S., 2009. "Characteristics and shock waves of supersonic two-phase flow of CO2 through converging- diverging nozzles," Doctoral Dissertation, Toyohashi University of Technology, Aichi, Japan.
[14] Joseph D, Yang B. Friction factor correlations for laminar, transition and turbulent flow in smooth pipes. Physica D 2010;239:1318-1328.
[15] Cicchitti A, Lombardi C, Silvestri M, Soldaini G, Zavattarelli R. Two-phase cooling experiments—pressure drop, heat transfer and burnout measurements. Energia Nucleare 1960;7:407–425.
[16] Redo M.A., Berana M.S., Espeña G.D., 2013. "Mathematical model of irreversible nozzle condition for heat-driven ejector refrigeration system," 8th Int'l. Conference on Multiphase Flow, Jeju, Korea.
[17] ASHRAE. Steam-Jet Refrigeration Equipment, Equipment Handbook, vol.13; 1979, pp. 13.1-13.6.
[18] ESDU, Ejectors and Jet Pumps, Design for Steam Driven Flow 1986, Engineering Science Data item 86030, Engineering Science Data Unit, London.
[19] Ouzzana M, Aidoun Z. Model development and numerical procedure for detailed ejector analysis and design. Applied Thermal Engineering 2003;23:2337-2351.
[20] Marynowski T, Desevaux P, Mercadier Y. Experimental and numerical visualizations of condensation process in a supersonic ejector. Journal of Visualization 2009:251-258.
[21] Daisuke S, Tanaka S, Yoshida K, Esashi M. Micro- ejector to supply fuel-air mixture to a micro-combustor. Sensors and Actuators 2005;119:528-536.
[22] Chou SK, Yang PR, Yap C. Maximum mass flow ratio due to secondary flow choking in an ejector refrigeration system. International Journal of Refrigeration 2009;24:486-499.
[23] Espeña G.D., 2014. "Heat-driven ejector refrigeration system for hot-spring resorts application," Master's Thesis, University of the Philippines Diliman.
[24] Sankarlal T, Mani A. Experimental investigations on ejector refrigeration system with ammonia. Renewable Energy 2007;32:1403–1413.
[25] Keenan H, Neumann EP, Lustwerk F. An investigation of ejector design by analysis and experiment. Journal of Applied Mechanics, ASME 1950;72;299-309.
[26] Selvaraju A, Mani A. Experimental investigation on R134a vapour ejector refrigeration system. Int. J. of Ref. 2006;29:1160-1166.